Cylindrical Inclusions in a Copolymer Membrane

Qiyi Zhang* and Yuqiang Ma

National Laboratory of Solid State Microstructures, Nanjing University, Nanjing 210093, China

Received: June 23, 2006; In Final Form: October 16, 2006

The membrane-mediated interaction between two parallel, cylindrical inclusions is investigated by using the self-consistent field theory (SCFT). The rodlike inclusions are located within the interior of the bilayer and are enveloped by two monolayers. They may exhibit one of the two basic types of behaviors involving pinching two monolayers together and swelling them outward. For different parameters, we calculate the density profile of the deformation membrane, the associated interaction free energy, as well as the conformational entropy of polymer chains. The similarity of the two types of interaction potentials is the qualitative characteristics. An energy barrier separates an attractive from a repulsive region; the repulsive region is preceded by a weak attraction at a large distance. The difference between them, which is due to the different contact environments around the rods, lies in the appearance of a small barrier at a short distance in the pinching structure. Particular emphasis is put on the closely energetic and entropic analyses of the interaction potential. We show that the chemical potential energy has provided a qualitative trend and roughly dominated the basic shape of the interaction potential; the amphiphile entropy in the swelling structure and the solvent entropy in the pinching structure, combined with the corresponding chemical potential energy, are responsible for the repulsive barrier at an intermediate distance and for the weak attraction at a large distance, respectively. The influence of inclusion hydrophobicity on the interaction potential is taken into account. In particular, the pinching and swelling structures can appear and can transform into each other in a system at intermediate hydrophobicity.

I. Introduction

Biological membranes with a variety of embedded or absorbed macromolecules and subsequent interactions between them have been studied intensively in recent years.[1,2] Examples for such macromolecules are transmembrane proteins[3−5] or peptides,[6,7] membrane-anchored polymers,[8] absorbed particles,[9] and rigid inclusions.[10,11] The interactions between membrane inclusions consist of direct interactions such as van der Waals, steric, or electrostatic forces and indirect interactions that are mediated by the membrane. The membrane-mediated interactions can be divided into static and dynamic interactions. The static interactions are due to perturbations of the equilibrium bilayer structure or shape. The dynamic interactions are mediated by shape fluctuations of the bilayer.[10] In the past, the static and indirect membrane-mediated interactions between inclusions have attracted great interest, and two different types of theoretical approaches have been presented. One is membrane elasticity theory,[12] and the other is chain packing theory.[13] The two models yield almost the same qualitative behavior of the membrane-mediated pair interaction potential; an energy barrier separates an attractive region from a repulsive region.

Whereas a number of previous studies have focused on absorbed, anchored, or transmembrane inclusions, no effort has been invested so far in detailed theoretical research concerning the inclusions sandwiched between the leaflets of the bilayer and the associated pair interactions. The exceptions are (i) the elastic theory treatment[14] of the responses of a membrane to localized forces and (ii) the two-dimensional density functional theory approach[15] of a rodlike inclusion inserted in a bilayer. In recent experiments,[16,17] after the "short" DNAs were microinjected locally to a part of a giant unilamellar vesicle, DNA-induced endocytosis was observed due to the DNA/lipid membrane local interactions. A possible mechanism for these interactions is that DNA encapsulation within an inverted micelle is included in the interior of the lipid membrane. The short DNAs can be considered as rigid rods 2.2 nm in diameter and 7.2 or 86.2 nm in length. The interactions of DNA/DNA and DNA/membrane have a principal effect on the characteristic sizes and shapes of the resulting endosomes. Another important field[18−20] is the artificial rigid-rod β-barrels with the inner diameter up to 2.5 nm, which are assembled from rigid-rod molecule scaffolds such as *p*-octiphenyl and function as synthetic ion channels and pores in a lipid bilayer membrane. Both the inner and the outer surfaces of the cylindrical β-barrels can be functionalized hydrophobically or hydrophilically.[20] In aqueous bilayer suspensions, one of the complex structures of the rigid-rod molecules and the rigid-rod β-barrels is their residences in the central location of the bilayer core.[19] The pair interactions of rigid-rod molecules or β-barrels and their corresponding energies are fundamental for understanding the self-assemblies of the rigid-rod objects and the multifunction of the synthetic pores.

Inclusions of this nature also include (i) the hairy-rod polymers deposited for the preparation of soft polymer cushions to support membranes,[21,22] (ii) vitamin E, ubiquinol, and ubiquinone as relatively small molecule natural antioxidants located within the hydrophobic core of the membrane bilayer,[23] (iii) the prion peptide PrP106−126, which is fully included into the hydrophobic region of the lipid bilayer and is roughly parallel to the membrane plane,[24] and (iv) the synthetic peptide nanotubes inserted into lipid bilayers to modulate the permeability properties of the cell wall.[25]

In a stack of regularly spaced membranes, there are two types of particulate inclusions[26−28] involving pinching neighboring membranes together and swelling them apart. The space extension of membrane deformation due to such an inclusion

10.1021/jp063951t CCC: $33.50
Published on Web 12/08/2006

is significantly included within a parabola region defined by $r^2 \simeq \lambda z$.[26] The vector $\mathbf{r}$ is in the equilibrium membrane plane (i.e., the $x-y$ plane in the present paper), which is normal to the z direction; $\lambda \equiv \sqrt{K/B}$, with K being the bending modulus and B being the compression modulus. As a result, the particle is enclosed and accompanied by the deformation parts of the membranes all of the time. The membrane-mediated pair interaction is attractive at large distances outside the parabola regions and is repulsive after the contact of the two parabolas.

The biomimetic bilayer membranes composed of amphiphilic polymers, as a system with no biological components exhibiting properties and processes similar to those occurring in natural biomembranes, have been used extensively[29,30] as model systems to study the physical properties of lipid bilayers by Monte Carlo simulation[31] and SCFT.[32] The components constituting the membrane, such as lipid tails or amphiphile polymers, are flexible and possess many possible conformations. This is an important factor underlying the interactions.[4] The SCFT successfully takes conformational entropy of the polymer chains into account. We will use a standard model of amphiphilic polymers, which we describe in the next section, and solve it within the framework of SCFT in order to theoretically explore the effect of rodlike inclusions residing in the interior of a single isolated bilayer membrane, with their orientation parallel to the membrane plane. Especially, the static membrane-mediated interactions between two identical and parallel rodlike inclusions will be studied and analyzed in detail in terms of the chain conformational entropies as well as the energies.

The paper is organized as follows. First in section II, we present a theoretical model for a bilayer membrane with embedded inclusions. Next in section III.A., we consider the influence of a single pinching or swelling rod on the membrane. We calculate the membrane deformation profile and the total free energy associated with this deformation and explain the energy difference between the two types of inclusions with the same radius. Finally, we extend this work in sections III.B. and III.C. to derive the indirect interactions between two identical parallel rodlike inclusions induced by the deformation of the membrane. We compare the two types of pair interaction potentials belonging to the pinching and swelling rods and present closely energetic and entropic analyses on the interaction potentials. The effect of the hydrophobicity of the cylindrical inclusions on the interaction energy profiles is also taken into account in section III.D.

II. The Models

The system consists of a copolymer−homopolymer mixture and one or two cylindrical inclusions. The incompressible mixture contains n_a amphiphilic diblock copolymers, composed of A (hydrophilic) and B (hydrophobic) monomers, and n_s solvent molecules, represented by hydrophilic homopolymers consisting of A segments only. All of the segments are defined based on a common segment volume ρ_0^{-1} and statical length b. All polymers are composed of N segments. A fraction, f, forms the hydrophilic block in the diblock. The interaction between hydrophobic and hydrophilic monomers is controlled by a local repulsion of strength χ, the usual Flory−Huggins parameter, with a choice of $\chi N = 30$ here.

The geometry of our two-dimensional model is described in Figure 1. In the absence of inclusions, the homogeneous bilayer membrane remains planar. It is immersed in a homopolymer solvent reservoir and located in the $x-y$ plane. The rigid cylindrical inclusion, characterized by the radius R, is embedded within the bilayer hydrophobic core with its long axis parallel to the membrane plane. The length of the cylindrical inclusion along the y-axis is assumed to be sufficiently larger than the linear dimension of a polymer chain in order to ignore the end effects of the cylinder, and the system can be treated as translationally invariant along the y-axis.

The surface of the cylindrical object is hard and impenetrable. The total segment density in the vicinity of and orthogonal to its surface drops to zero in a boundary region of width ϵ according to[33−35]

$$\phi_0(\mathbf{r}) = \begin{cases} 0, & r \le R, \\ \frac{1}{2}\left\{1 - \cos\left(\frac{\pi(r-R)}{\epsilon}\right)\right\}, & R \le r \le R+\epsilon, \\ 1, & \text{else}, \end{cases} \quad (1)$$

where ϵ is chosen to be much smaller than R_g, the polymer radius of gyration.

The contact interaction potential $H(\mathbf{r})$, which acts on the monomers close to the cylinder, is modeled as[33−36]

$$\frac{H(\mathbf{r})}{\chi N} = \begin{cases} \infty, & r \le R, \\ \Lambda\left\{1 + \cos\left(\frac{\pi(r-R)}{\epsilon}\right)\right\}, & R \le r \le R+\epsilon, \\ 0, & \text{else}, \end{cases} \quad (2)$$

where Λ controls the strength of the field at the cylindrical obstacle surface. $\Lambda = 0$ means a neutral rod surface. A negative value of Λ corresponds to a hydrophilic interaction, while a positive one indicates a hydrophobic interaction.

Within the well-established SCFT, the boundary conditions are needed. For the four boundaries of our simulation box, the Neumann condition is used. At the boundary on the rod, the Dirichlet condition is used because a polymer cannot cross the hard rod surface. In the grand canonical ensemble,[32,37−39] the free-energy functional has the form

$$\begin{aligned} \frac{N\mathcal{F}}{\rho_0 k_B T V} = & -\frac{1}{V}Q_s - \frac{\exp(\mu/k_B T)}{V}Q_a \\ & + \frac{1}{V}\int d\mathbf{r}\chi N[\phi_T(\mathbf{r})\phi_H(\mathbf{r}) + \phi_S(\mathbf{r})\phi_T(\mathbf{r})] \\ & + \frac{1}{V}\int d\mathbf{r}H(\mathbf{r})[\phi_H(\mathbf{r}) + \phi_S(\mathbf{r}) - \phi_T(\mathbf{r})] \\ & - \frac{1}{V}\int d\mathbf{r}[w_H(\mathbf{r})\phi_H(\mathbf{r}) + w_T(\mathbf{r})\phi_T(\mathbf{r}) + \\ & \qquad w_S(\mathbf{r})\phi_S(\mathbf{r})] \\ & + \frac{1}{V}\int d\mathbf{r}\xi(\mathbf{r})[\phi_H(\mathbf{r}) + \phi_T(\mathbf{r}) + \phi_S(\mathbf{r}) - \phi_0(\mathbf{r})] \end{aligned} \quad (3)$$

Here μ is the relative chemical potential of the amphiphile. Because of an assumed incompressibility constraint, there is only one independent chemical potential. The local volume fractions of the A (head) and B (tail) segments of the amphiphile are given by $\phi_H(\mathbf{r})$ and $\phi_T(\mathbf{r})$, respectively. Likewise, $\phi_S(\mathbf{r})$ is the local concentration of solvent. We let $w_H(\mathbf{r})$ denote the value of the mean field felt by the head segments at $\mathbf{r}$, $w_T(\mathbf{r})$ is the field for the tail segments, and $w_S(\mathbf{r})$ is the field for the solvent segments. The Q_s and Q_a are the single chain partition functions of the solvent and amphiphile molecules, respectively, subjected

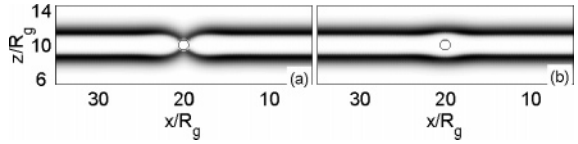

Figure 1. Density distributions of the membrane in the vicinity of a neutral rodlike inclusion with $R = 0.6R_g$, $f = 0.4$, and $\mu/k_BT = 3.9120$. For convenience, all of the density distributions in the present paper follow the same color rule; a decreasing segment density is denoted as a color map from black to white. In this picture, the hydrophilic segments are dark; between them are hydrophobic segments, and outside of them are the solvent segments. The area enclosed by the small dark circle represents the cross section of the rod. (a) Pinching rod. (b) Swelling rod.

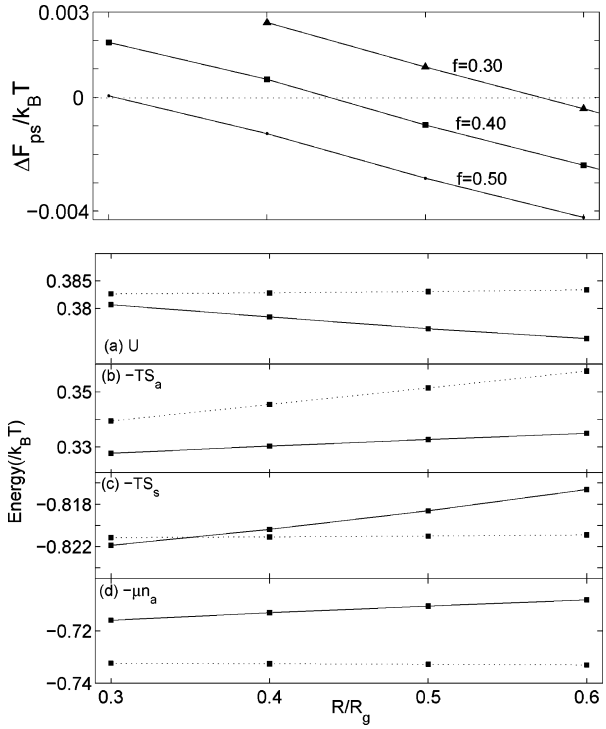

Figure 2. (Top graph) The free energy difference, ΔF_{ps}, as a function of radius, R, calculated at $\mu/k_BT = 3.9120$ and $\Lambda = 0$ for several different values of the amphiphile's hydrophilic fraction, f. (Bottom graph) The individual contributions to ΔF_{ps} as a function of R, calculated at $\mu/k_BT = 3.9120$ and $f = 0.4$. The solid and dotted curves denote the results of the pinching rod and swelling rod, respectively.

to the above fields. A Lagrange multiplier field $\xi(\mathbf{r})$ is introduced to enforce incompressibility.

III. Results

Our results are focused on the following set of system parameters: $\mu/k_BT = 3.9120$, and $R = 0.5R_g$, $1.0R_g$, $1.5R_g$, and $2.0R_g$. The membrane thickness is $3.6R_g$ with different hydrophobic thicknesses of $2.52R_g$, $2.16R_g$, and $1.80R_g$, corresponding to $f = 0.3$, 0.4, and 0.5, respectively. In the following, we are interested in the variations of the distance, d, between the front surfaces of the rods, of the amphiphile architecture, f, and of the rod radius, R. The surface of each rod facing another approaching rod is called the front surface, and the other is the rear surface. In order to discuss the rod/rod interaction mediated by the membrane, it is necessary to first examine the interaction between the membrane and a single isolated cylinder.

A. Single Isolated Cylindrical Inclusion. We first illustrate the membrane deformation due to a single isolated rodlike inclusion by means of two cases: (i) pinches two leaflets of the same bilayer together or (ii) pushes them apart, forming a local bulge. Both the pinching and the swelling inclusions are shown in Figure 1 for the same rod and membrane. As we know, hydrophobic objects may be enclosed within the bilayer interior, protected by the hydrophilic heads. We pose the following questions. What is it about a neutral inclusion (e.g., a neutral colloid, a neutral rod inclusion discussed here, etc.) embedded in a bilayer membrane, and within the same membrane, is a pinching or a swelling inclusion energetically favorable? We compare the free energies of the pinching and swelling structures for the same neutral rod in the same bilayer with an artificially "biased" structure, in which we confine the rod inclusion by requiring that it acts as a pinching or a swelling inclusion.[32,34] The answer is presented in the top graph of Figure 2. $\Delta F_{ps}(R)$ is the free energy difference between the pinching and swelling structures as a function of the rod radius R. It is given by

$$\Delta F_{ps}(R) = \mathscr{F}_p(R) - \mathscr{F}_s(R) \tag{4}$$

where $\Delta F_{ps} < 0$ means a more favorable pinching structure.

We point out an important feature of ΔF_{ps}: a larger R is required to satisfy $\Delta F_{ps} < 0$ for a smaller f because a smaller f corresponds to a larger membrane tail core thickness. For example, the radius favoring a pinching structure is $R \geq 0.5R_g$ for $f = 0.4$. We will analyze the rod−membrane interaction, ΔF_{ps}, based on this typical case in the bottom graphs of Figure 2.

In order to correctly interpret the interaction behavior, the enthalpy energy, U, amphiphile entropy, S_a, solvent entropy, S_s, and chemical potential energy, $-\mu n_a$, are obtained by separating the free energy as[37]

$$\mathscr{F} = U - T(S_s + S_a) - \mu n_a \tag{5}$$

The bottom graphs of Figure 2 display the four contributions to ΔF_{ps} as a function of rod radius for the same bilayer. The rodlike inclusion embedded within a bilayer interior provides a confined environment for the polymer chains. The different confined environments determine the characteristics of the ΔF_{ps} curves and, furthermore, predict the distinct features of the membrane-mediated rod/rod interactions. The pinching rod contacts and confines the amphiphile and solvent molecules, while the swelling rod only keeps in contact with the tail chains. Hence, at constant R, the pinching S_a is larger than the swelling S_a, while the pinching S_s has a smaller value except in the case of $R = 0.3R_g$. This case originates from the more space available for solvents. The head groups of two monolayers highly bend toward the rod because of its small radius and, subsequently, shield the solvents from contact with the rod surface. Similarly, the swelling structure needs more amphiphiles to line the rod, while the pinching structure forces more amphiphiles to leave the membrane. This is the reason that the n_a and U of the swelling state are larger than those of the pinching state. Also, the hydrophobic/hydrophilic interfacial area, which is effectively increased in the former case and reduced in the latter case, contributes to U.

B. Interaction between Two Swelling Cylindrical Inclusions. The quantity of greatest interest in the present work is $F(d)$, the membrane-mediated interaction free energy between two rods at distance d from each other,

$$F(d) = \mathscr{F}(d) - \mathscr{F}(\infty) \tag{6}$$

where the reference state is taken to be the state where the two rods are separated far enough so that they do not feel each other.

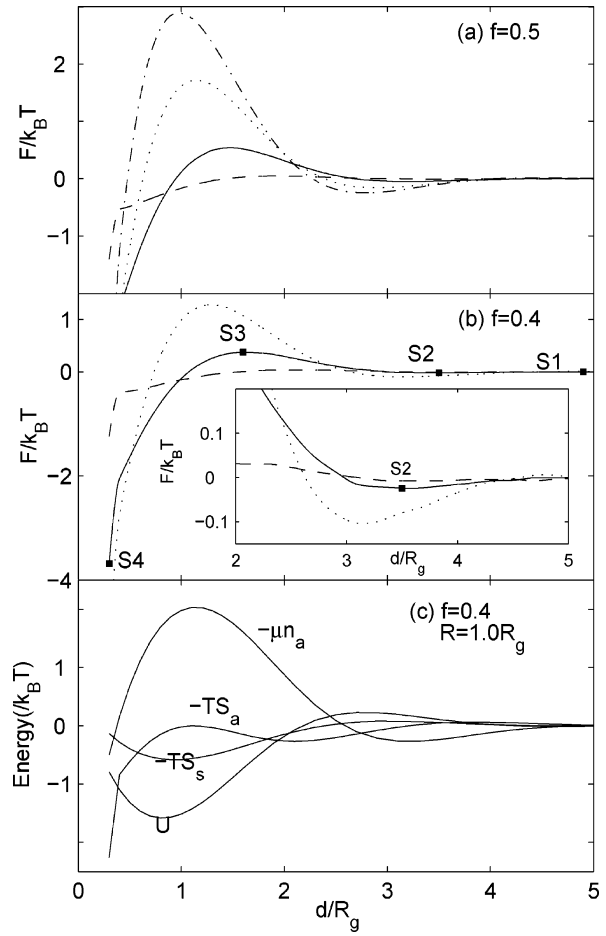

Figure 3. The interaction free energy, F, between two swelling rods as a function of d, with $\mu/k_BT = 3.9120$ and $\Lambda = 0.5$, for $f = 0.5$ (a) and $f = 0.4$ (b). Results are presented for $R = 0.5R_g$ (dashed line), $R = 1.0R_g$ (solid line), $R = 1.5R_g$ (dotted line), and $R = 2.0R_g$ (dash-dotted line). The inset presents an enlarged view of the weak attraction. We identify different states of the solid curve by filled squares labeled s1−s4. (c) The individual contributions to F plotted together as a function of the separation, d, calculated at $\mu/k_BT = 3.9120$, $f = 0.4$, and $R = 1.0R_g$.

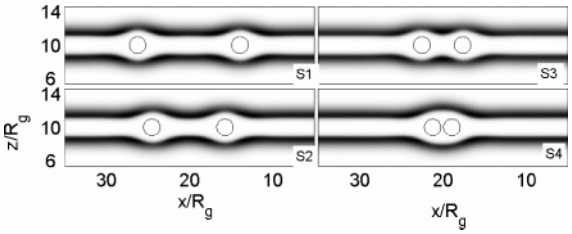

Figure 4. Density plots of the membrane containing two parallel swelling rods with the same radius, $R = 1.0R_g$, at $f = 0.4$, $\mu/k_BT = 3.9120$, and $\Lambda = 0.5$. The four graphs correspond to the states marked by the filled squares in Figure 3.

Figure 3a,b shows $F(d)$ of two swelling rods for various values of the rod radius, R, at a constant hydrophobic strength of $\Lambda = 0.5$. All of the curves exhibit the same qualitative and nonmonotonic behavior; an energy barrier (e.g., the s3 state) separates an attractive region from a repulsive region, and an energy minimum (e.g., the s2 state) precedes the repulsive region.

The density distributions of the deformation membrane are illustrated in Figure 4 for $R = 1.0R_g$. The four states correspond to the positions labeled s1−s4 in the $F(d)$ curve of Figure 3b. The membrane, which hosts inclusions, is divided into two parts, the relatively "free" part and the perturbed part in the vicinity of the invasive rods. The perturbed part is similar to the parabola region induced by particles residing in a stack of membranes.[26] Moreover, through the whole approaching process, the system remains symmetric under reflection in the bilayer midplane and under reflection in the perpendicular midplane between the two rods. Namely, the deformation environments around the two rods are always kept similar. Particularly, as long as the two rods are far apart (e.g., the s1 state), the front and rear deformation environments of a rod are symmetric. During the process of the two rods approaching each other, the two front membranes are heavily squeezed while the two rear membranes remain slightly "growing". Accordingly, the two front membranes are more sensitive to confinement and mainly contribute to the interaction potential.

We can understand the source of the effective interaction, F, by means of its various contributions, which are described in eq 5 and plotted together in Figure 3c for the convenience of examining their relative magnitudes. As a typical example, only the case of $R = 1.0R_g$ is shown in Figure 3c. Clearly, the qualitative trend and basic shape of the F curve are roughly attributed to the combination of the chemical potential energy and the amphiphile entropy energy.

We first focus on the gentle depletion attraction at a large separation (from s1 to s2) and the steep depletion attraction at a very short distance (from s3 to s4). The former attractive region is partially caused by the escape of the free amphiphiles from between the two rods; the perturbed membrane around the rods almost has not been squeezed. The latter depletion attraction is induced by the release of the amphiphiles inside the perturbed parts of the membrane. The perturbed parts overlap, and the two rods come into full contact with their behavior being similar to the effect of a single rod (see s4 in Figure 4). Both depletions provide more room for amphiphiles and thus need more amphiphile chains.

Between the two depletion attractions, a repulsive region at an intermediate separation (from s2 to s3) has to be experienced. In the repulsive region, the two front membranes are squeezed together more and more seriously, forcing amphiphiles to leave the membrane, which leads to large losses in the amphiphile entropy and in the amount of amphiphiles.

To a large extent, the internal energy U is simply proportional to the interfacial area and roughly proportional to the amount of amphiphile in our system. Thus, U has similar shape to $-\mu n_a$ but with an opposite sign. In the present system, the rods are always kept within the interior of the bilayer. The bulge of the membrane, induced by the swelling rods, means the reduction of the space available for solvents, to a certain degree. Hence, S_s exhibits a qualitatively contrary behavior to S_a.

Returning to Figure 3a,b, increasing R results in heavier swelling deformations of the two monolayers, which are expressed in interaction potentials as higher barriers and lower energy minima (around s2). The interaction energy curve for $f = 0.4$ and $R = 2.0R_g$ is not shown in Figure 3b and will be discussed in Figure 8 of section III.D.

C. Interaction between Two Pinching Cylindrical Inclusions. Figure 5a,b displays the interaction free energy $F(d)$ of two pinching rods for various values of rod radius, R, at fixed $\Lambda = 0$. The membrane and the solvent distributions of the states, labeled p1−p6, are shown in Figure 6. Figure 5c illustrates the four energy contributions to F for the case of $R = 1.0R_g$.

We analyze the interaction potential in three stages. In the first stage, roughly from p1 to p2, the two rods approach each other from far away; the middle isolated membrane is squeezed

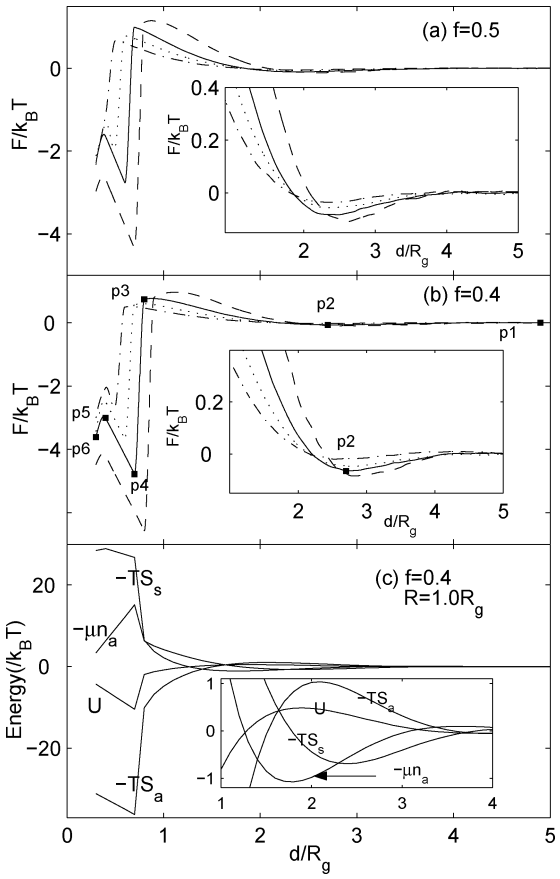

Figure 5. The interaction free energy, F, between two pinching rods as a function of d, with $\mu/k_BT = 3.9120$ for $f = 0.5$ (a) and $f = 0.4$ (b). Profiles are shown for $R = 0.5R_g$ (dashed line), $R = 1.0R_g$ (solid line), $R = 1.5R_g$ (dotted line), and $R = 2.0R_g$ (dash-dotted line). The insets show enlarged views of the corresponding weak attractions. Different states of the solid curve are identified by filled squares labeled p1−p6. (c) The individual contributions to F plotted together as a function of d, calculated at $\mu/k_BT = 3.9120$, $f = 0.4$, and $R = 1.0R_g$. The inset provides an enlarged view of the four contributions.

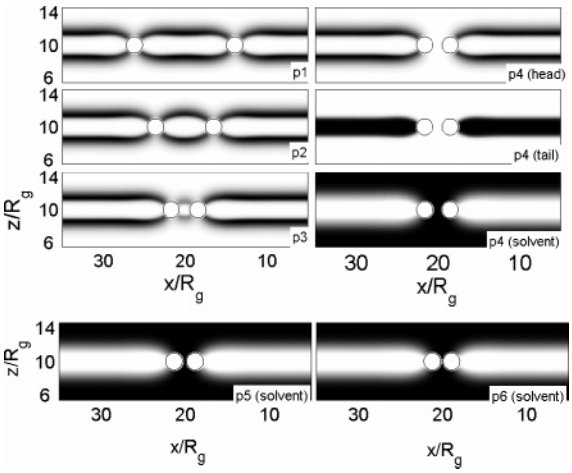

Figure 6. Density profiles of the membrane containing two parallel pinching rods with the same radius $R = 1.0R_g$, at $f = 0.4$ and $\mu/k_BT = 3.9120$. The six states correspond to the states marked by the filled squares in Figure 5. We depict the density distributions of the head, tail, and solvent segments of the p4 state; p5 and p6 states are expressed using their distributions of solvent segments.

more and more heavily and forced to release some copolymers and thus has to endure large losses of n_a, S_a, and U. However, the losses of n_a and U are outweighed by their rises in the two isolated rear membranes. The S_a, as discussed above, is sensitive to the confined environment provided by the two rods. So, the reduction of S_a in the mid-membrane dominates the trend of the total S_a. Lowering the content of the amphiphiles in the mid-membrane causes more homopolymer to penetrate the monolayers; thus, S_s increases.

The short-range attraction (around p2) has its origin in the combination of $-\mu n_a$ and $-TS_s$, as is evident in the inset of Figure 5c. Comparably, in the above case of the swelling rods, the weak attraction (around s2) partially results from the depletion of the free amphiphiles ($-TS_a$). Indeed, there is a slight increase in the S_a curve at a large d, but the effect of this rise is completely swamped by the other energy components.

The second stage is from p2 to p4. As d decreases further, the amount of amphiphiles of the mid-membrane is reduced rapidly until the mid-membrane fully escapes out from between the two front rods and is substituted by the emergence of solvents. The three sub-membranes merge into two rear membranes. The structure transition from p3 to p4 appears, which can be seen from the head, tail, and solvent density distributions of the p4 state. This transition is accompanied by abrupt jumps in the physical quantities. For example, a steep depletion in S_a is induced by the smaller and smaller mid-membrane; more and more solvents come into contact with the two rods, interact with both surfaces, and experience a large loss of conformational entropy. The rapid reduction of n_a in the mid-membrane offsets the increase in the two "growing" rear membranes; the total n_a decreases. This is also responsible for the reduction of U. The $-\mu n_a$ and $-TS_s$ combine to give a strong repulsion in this stage.

The last stage is the short distance from p4 to p6. An interesting phenomenon is the interaction behavior; a steep depletion region (after p5) is preceded by a sharp repulsive region (p4 to p5). This is quite different from the swelling rods at corresponding separations. After the p4 state, the solvents are confined and squeezed by the two rods, thus experiencing a large conformational entropy loss. Until the two rods come into full contact (e.g., see p6), a depletion attraction induced by the solvents occurs. Without the mid-membrane, the two rear membranes look as if they are being pinched and elongated by the two approaching rods, and thus S_a decreases. Naturally, the growths of the two rear membranes cause rises in n_a and U.

Returning to Figure 5a,b, increasing R leads to a smaller mismatch between the rod diameter and the membrane thickness and, thus, to a smaller local deformation of the membrane, which is different from the case of the swelling rod. The consequence lies in two aspects. One is the lower barrier (the maximum of F; e.g., see p3) because of weaker deformation. The other is the shorter distance (e.g., after p4) between two rods where only the solvents are confined. This is because of the longer depletion distance needed by the weaker deformation mid-membrane.

To clearly understand the interaction behavior of the two types of inclusions, we give a qualitative comparison of their physical mechanisms. At large and intermediate separations, all of the rod/rod interactions have qualitatively the same features; a long-range repulsion is preceded by a short range attraction. At short separations, they have different properties. The swelling rod/rod interaction is featured by a steep depletion attraction; the pinching interaction is characteristic of a sharp repulsive region followed by a steep depletion region. Underlying the two types of interactions are different physical natures. Roughly speaking, the qualitative trend and feature of the pinching interaction potential are attributed to the combination of $-\mu n_a$ and $-TS_s$ at large and intermediate separations. The swelling interaction

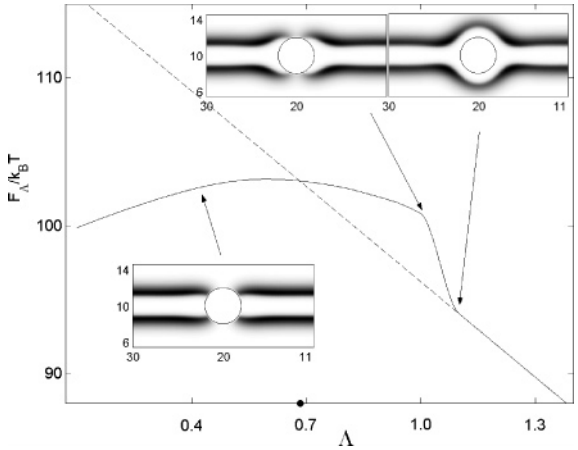

Figure 7. The free energy of the pinching structure (solid line) and the swelling structure (dashed line) as a function of the surface field, Λ. The calculations correspond to $f = 0.4$, $\mu/k_BT = 3.9120$, and $R = 2.0R_g$. A filled circle indicates the "crossover" value of Λ.

potential is shaped by the combination of $-\mu n_a$ and $-TS_a$ at all separations. In the two types of interactions, the most significant term, $-\mu n_a$, has roughly a similar shape but with an opposite sign to U because both track the copolymer concentrations by and large. The $-TS_a$ and $-TS_s$ also have similar shapes with opposite signs, except after the mid-membrane disappearance due to structure transition in the pinching interactions.

We stress that the various ambient environments of the rod provide different sources of interaction and thus different interaction properties. During the process of approaching each other, the two swelling rods are always fully enclosed by tails, even in close contact. This property maintains the integrity of the whole membrane (i.e., the two front membranes and the two rear membranes are always kept in connectivity). Oppositely, the two pinching rods are always kept in contact with the three components, the heads, the tails, and the solvents, but are kept far away from each other. This divides the membrane into three small isolated sub-membranes, the two rear membranes and the middle membrane.

D. Influence of the Hydrophobicity to Interaction. Figure 7 shows the free energy of the pinching and swelling states as a function of the rod surface hydrophobicity, Λ. The free energy F_Λ is shifted up by the free energy of the bilayer system without inclusion. Figure 8 shows how the surface hydrophobicity affects $F(d)$. Both of the diagrams are derived for $R = 2.0R_g$, $f = 0.4$, and $\mu/k_BT = 3.9120$.

From Figure 7, we are able to compare the relative stabilities of the pinching and swelling geometries over a wide range of hydrophobicities. As expected, the swelling state is favored for large Λ; the pinching state is favorable under weak hydrophobicity, without formation in sufficiently large Λ at all. In the intermediate Λ, a transition from the pinching to the swelling structure will take place when the surface potential exceeds a certain crossover value, which depends on the rod size as well as the membrane characteristics, such as the architectural parameter and chemical potential.

In the intermediate hydrophobic case, such as $\Lambda = 1.0$, a large barrier, with a height up to $10k_BT$ and a width of approximately $1.6R_g$, appears in the $F(d)$ curve of Figure 8. It can be seen from s2′ and s3′ in Figure 9 that the hydrophobicity is too weak to maintain the rod's full enclosure within the bilayer interior. The membrane is squeezed heavily by the two rods to rupture into three sub-membranes, and the rods are partially exposed to solvents without the shield of the two monolayers. This pinching geometry is of larger free energy than the swelling

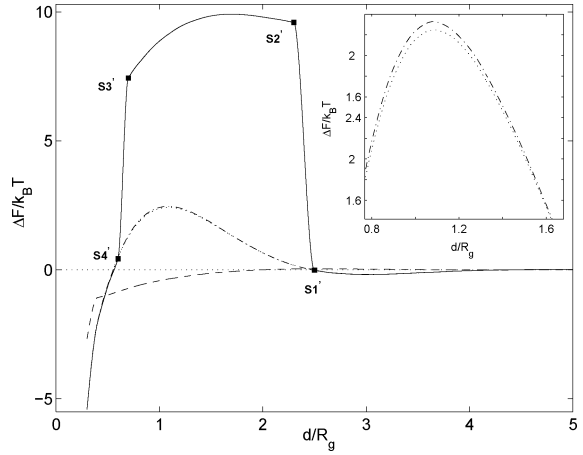

Figure 8. The interaction free energy, F, between two swelling rods as a function of d, with $\mu/k_BT = 3.9120$, $f = 0.4$, and $R = 2.0R_g$, for different strengths of hydrophobicity, Λ. The dashed, solid, dotted, and dash-dotted lines correspond to the values of $\Lambda = 0.5$, 1.0, 1.5, and 2.0, respectively. Observe that the dotted and dash-dotted lines almost overlap, which are partially shown as an enlarged view in the inset. Different states of the solid curve are identified by the filled squares labeled s1′−s4′.

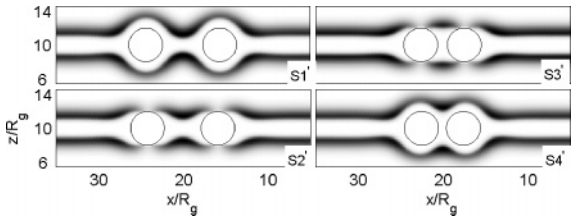

Figure 9. Concentration distributions of the membrane containing two parallel swelling rods with the same radius $R = 2.0R_g$ at $f = 0.4$, $\mu/k_BT = 3.9120$, and $\Lambda = 1.0$. The four states correspond to the states marked by the filled squares in Figure 8.

geometry, as is evident in Figure 7. At a short separation (see state s4′), the deformation extent of the membrane is reduced. The three sub-membranes coalesce into an integral membrane, and the rod is shielded again, as in the case of a large separation (see state s1′).

In the weak hydrophobic case, such as $\Lambda = 0.5$, the system prefers the pinching structure, whose pair interaction energy is, in fact, shown in the dashed line of Figure 8. Accordingly, within the same membrane, the behavior of the interaction profile of the hydrophobic pinching rod is similar to that of the equal-sized, neutral pinching rod (i.e., the dash-dotted line in Figure 5b). However, the hydrophobicity of $\Lambda = 0.5$ enlarges the effective rod radius, which results in some differences at a short distance.

In the large hydrophobic case, such as $\Lambda \geq 1.5$, the system recovers the case discussed in section III.B. (i.e., the rod is fully enveloped by two monolayers), and the $F(d)$ curves are qualitatively and quantitatively similar.

In summary, depending on the different values of the hydrophobicity, the membrane-hosting hydrophobic rod may be characteristic of a swelling structure, a pinching structure, or even the crossover between them.

IV. Summary and Concluding Remarks

We have studied theoretically the behavior of cylindrical inclusions embedded within the interior of a copolymer bilayer membrane, particularly, the membrane-mediated interaction between two rodlike inclusions. This interaction is analyzed in terms of three energy components: the interfacial energy, the

entropy energy, and the chemical potential energy. Our analysis suggests that the conformational entropy of the polymer chains is a direct contribution to the repulsive barrier and the weak attraction, and the chemical potential energy dominates the qualitative trend of the interaction energy. The influence of rod hydrophobicity on the interaction potential is also taken into account. In the intermediate hydrophobic range, a very large barrier appears in the interaction potential.

By using a field-theoretic method, we can incorporate many important physical details, such as the conformational properties of the polymer chains. Our results of the interaction potential behavior of two swelling rods are qualitatively similar to that of two transmembrane proteins. The similarity is due to, qualitatively, the same local deformation of the membrane induced by the integral protein with a hydrophobic mismatch as that induced by the present cylinderlike inclusion. Moreover, our mean-field method outlined in this paper can be easily extended to account for the two-body interaction characteristics in the cases of transmembrane proteins with a hydrophobic mismatch, membrane-absorbed particles, and a system of a spherical particle and a membrane.

Acknowledgment. Q.Z. would like to acknowledge helpful discussions with Dr. Qing Liang. This work was supported by the National Natural Science Foundation of China, No. 10334020, No. 10021001, and No. 10574061.

Supporting Information Available: Details of the SCFT methodology and the formulas of the free energy components are provided. This material is available free of charge via the Internet at http://pubs.acs.org.

References and Notes

(1) Dan, N.; Pincus, P.; Safran, S. A. *Langmuir* **1993**, *9*, 2768.
(2) Biscari, P.; Bisi, F. *Eur. Phys. J. E* **2002**, *7*, 381.
(3) Kik, R. A.; Leermakers, F. A. M.; Kleijn, J. M. *Phys. Chem. Chem. Phys.* **2005**, *7*, 1996.
(4) May, S. *Langmuir* **2002**, *18*, 6356.
(5) Nielsen, C.; Goulian, M.; Andersen, O. S. *Biophys. J.* **1998**, *74*, 1966.
(6) Huang, H. W.; Chen, F. Y.; Lee, M. T. *Phys. Rev. Lett.* **2004**, *92*, 198304.
(7) Zemel, A.; Ben-Shaul, A.; May, S. *Eur. Biophys. J.* **2005**, *34*, 230.
(8) Sens, P.; Turner, M. S. *Biophys. J.* **2004**, *86*, 2049.
(9) Koltover, I.; Rädler, J. O.; Safinya, C. R. *Phys. Rev. Lett.* **1999**, *82*, 1991.
(10) Weikl, T. R. *Phys. Rev. E* **2002**, *66*, 061915.
(11) Weikl, T. R. *Eur. Phys. J. E* **2003**, *12*, 265.
(12) Bohinc, K.; Kralj-Iglič, V.; May, S. *J. Chem. Phys.* **2003**, *119*, 7435.
(13) May, S.; Ben-Shaul, A. *Phys. Chem. Chem. Phys.* **2000**, *2*, 4494.
(14) Turner, M. S.; Sens, P. *Biophys. J.* **1999**, *76*, 564.
(15) Frink, L. J. D.; Frischknecht, A. L. *Phys. Rev. E* **2005**, *72*, 041923.
(16) Angelova, M. I.; Hristova, N.; Tsoneva, I. *Eur. Biophys. J.* **1998**, *28*, 142.
(17) Angelova, M. I.; Tsoneva, I. *Chem. Phys. Lipids* **1999**, *101*, 123.
(18) Weiss, L. A.; Sakai, N.; Ghebremariam, B.; Ni, C.; Matile, S. *J. Am. Chem. Soc.* **1997**, *119*, 12142.
(19) Sakai, N.; Matile, S. *Chem. Commun.* **2003**, 2514.
(20) Sakai, N.; Mareda, J.; Matile, S. *Acc. Chem. Res.* **2005**, *38*, 79.
(21) Sackmann, E. *Science* **1996**, *271*, 43.
(22) Wiegand, G.; Jaworek, T.; Wegner, G.; Sackmann, E. *Langmuir* **1997**, *13*, 3563.
(23) Afri, M.; Ehrenberg, B.; Talmon, Y.; Schmidt, J.; Cohen, Y.; Frimer, A. A. *Chem. Phys. Lipids* **2004**, *131*, 107.
(24) Grasso, D.; Milardi, D.; Rosa, C. L.; Rizzarelli, E. *New J. Chem.* **2001**, *25*, 1543.
(25) Chipot, C.; Tarek, M. *Phys. Biol.* **2006**, *3*, S20.
(26) Sens, P.; Turner, M. S.; Pincus, P. *Phys. Rev. E* **1997**, *55*, 4394.
(27) Subramanian, G.; Hjelm, R. P.; Deming, T. J.; Smith, G. S.; Li, Y.; Safinya, C. R. *J. Am. Chem. Soc.* **2000**, *122*, 26.
(28) Sens, P.; Turner, M. S. *Eur. Phys. J. E* **2001**, *4*, 115.
(29) Srinivas, G.; Discher, D. E.; Klein, M. L. *Nano. Lett.* **2005**, *5*, 2343.
(30) Taubert, A.; Napoli, A.; Meier, W. *Curr. Opin. Chem. Biol.* **2004**, *8*, 598.
(31) Müller, M.; Schick, M. *J. Chem. Phys.* **1996**, *105*, 8282.
(32) Katsov, K.; Müller, M.; Schick, M. *Biophys. J.* **2004**, *87*, 3277.
(33) Matsen, M. W. *J. Chem. Phys.* **1997**, *106*, 7781.
(34) Lee, J. Y.; Shou, Z.; Balazs, A. C. *Phys. Rev. Lett.* **2003**, *91*, 136103.
(35) Müller, M.; Binder, K. *J. Phys.: Condens. Matter* **2005**, *17*, S333.
(36) Li, W.; Wickham, R. A.; Garbary, R. A. *Macromolecules* **2006**, *39*, 806.
(37) (a) Thompson, R. B.; Matsen, M. W. *J. Chem. Phys.* **2000**, *112*, 6863. (b) Zhang, Q.; Ma, Y. *J. Chem. Phys.* **2006**, *125*, 164710.
(38) Matsen, M. W. *J. Chem. Phys.* **1999**, *110*, 4658.
(39) Matsen, M. W. *Phys. Rev. Lett.* **1995**, *74*, 4225.